Title

Evaluation of faults stability due to passing seismic waves: Study case of groundwater level changes induced by the 2011 Tohoku earthquake in Central Japan

Authors

Jeanne, Pierre

Guglielmi, Yves

Rutqvist, Jonny

et al.

Publication Date

2021-12-01

DOI

10.1016/j.hydroa.2021.100103

Peer reviewed

Evaluation of faults stability due to passing seismic waves: study case of groundwater level changes induced by the 2011 Tohoku earthquake in Central Japan

Pierre Jeanne[1], Yves Guglielmi[1], Jonny Rutqvist[1]

Takanori Kunimaru[2] and Hiroyuki Umeki[2]

[1] Lawrence Berkeley National Laboratory, Energy Geoscience Division, Berkeley, CA, 94720, USA.

[2] Nuclear Waste Management Organization of Japan (NUMO), Mita NN Bldg. 2F, 4-1-23 Shiba, Minato-ku, Tokyo

Abstract

In the study, we analyze changes in groundwater pressure observed in several boreholes drilled in and around the Mizunami Underground Research Laboratory (MIU) induced by the 2011 off the Pacific coast of Tohoku Earthquake (Mw 9.0).The aim of this project is a development of methodology to evaluate systematic fault activity by numerical analysis. To reach this goal we investigate the behavior of the fault zones present in the area during the passing of seismic waves. We built a simplified hydrogeological model of the MIU site and performed a series of fluid flow simulations with TOUGH2 flow numerical code. We investigate how changes in permeability along three faults present in the study area: the Tsukiyoshi Fault, the Hiyoshi Fault and the Main-Shaft Fault may have influence the groundwater level monitored in boreholes intervals. We also test the influence of the cone of depression at the MIU site and the hydraulic connectivity between the sedimentary cover and the granite aquifers. Our results suggest that two main mechanisms are responsible for the observed changes in groundwater pressure: (1) crustal dilation induced by the Tohoku earthquake causing a groundwater recharge from the sedimentary aquifers to the Toki granite aquifer where the sedimentary cover is thick; and (2) permeability increase along faults critically oriented for shear reactivation and oriented in the direction of the passing seismic wave. In this case, the seismic wave increases the shear stress acting on the fault promoting slip and a

change in permeability through a mechanism of slip-induced dilation. Faults not critically stressed and faults critically oriented for shear reactivation but oriented perpendicular to the passing seismic wave are not reactivated.

1. Introduction

Groundwater level changes caused by earthquakes have been investigated since the 1930s (Leggette and Taylor 1935; Blanchard and Byerly, 1935). Since then, the response of groundwater levels to earthquakes has been widely observed and documented (Wang and Manga, 2010). Two types of co- and post-seismic responses are usually recorded in groundwater levels: water-level oscillation (Blanchard and Byerly, 1935; Cooper et al., 1965; Liu et al., 1989; Kitagawa et al., 2011) and step-like rises or falls (Wakita 1975; Quilty and Roeloffs, 1997), and sustained gradual rises or falls for several days or weeks (Matsumoto, 1992; Roeloffs, 1998; Brodsky et al., 2003; Wang and Chia, 2008, Niwa et al., 2012). The mechanism of the latter type is uncertain. Several processes were proposed to explain these changes depending on the distance to the earthquake location.

- In the near field of an earthquake, water level changes can be explained by poroelastic pressure response to the earthquake's static strain field (Wakita, 1975; Quilty and Roeloffs, 1997; Jonsson et al., 2003) with groundwater changes proportional to volumetric strain (Quilty and Roeloffs, 1997). The water level rises in contraction zones and falls in regions of dilation (King et al., 1999; Lee et al., 2002; Wang and Manga, 2010).

- In the intermediate and far fields, earthquake-induced groundwater level changes may result from the shaking of the rock by seismic waves and leading to an increase in permeability (Rojstaczer and Wolf, 1992; Piombo et al., 2005; Elkhoury et al., 2006; Geballe et al., 2011; Shi et al., 2013; Sun et al., 2015; Xue et al., 2016). This increase may be caused by: the removal of gas from the pore space (Linde et al., 1994; Matsumoto and Roeloffs, 2003), the fracturing of solid rocks (Shi and Wang, 2016) and the

removal of barriers clogging the groundwater flow (Brodsky et al., 2003).

These changes in hydraulic properties of the geological rock formations can enhance basin-wide fluid transport extending to depths of a few kilometers. This can have important implications in particular for geologic disposal of radioactive waste, where the performance depends on the integrity of the natural system to contain radionuclides for tens of thousands of years. It is thus of crucial interest to nuclear waste authorities that the permeability changes in response to earthquakes can be better understood and eventually be predicted with confidence. It is particularly important in a country like Japan, where faulting is so ubiquitous that repository sites are expected to be co-located with a number of fault zones. In the study, we analyze changes in groundwater pressure observed in several boreholes drilled in and around the Mizunami Underground Research Laboratory (MIU) induced by the 2011 off the Pacific coast of Tohoku Earthquake (Mw 9.0). These groundwater pressure changes were fully described in Niwa et al (2012). They proposed that co-seismic changes of groundwater pressure could have resulted from (i) crustal dilation/contraction induced by earthquakes, (ii) permeability increase along local geological structures such as impermeable faults and (iii) by the complex hydraulic perturbations around the laboratory shafts. Here, we analyze more deeply the behavior of the local faults and the difference in hydraulic properties between the different geological layers through numerical simulations with the fluid flow simulator TOUGH2 (Pruess et al., 2011). The goal is to better characterize the causes of the monitored groundwater pressure to understand the behavior of the fault zones during the propagation of seismic waves due to remote earthquakes.

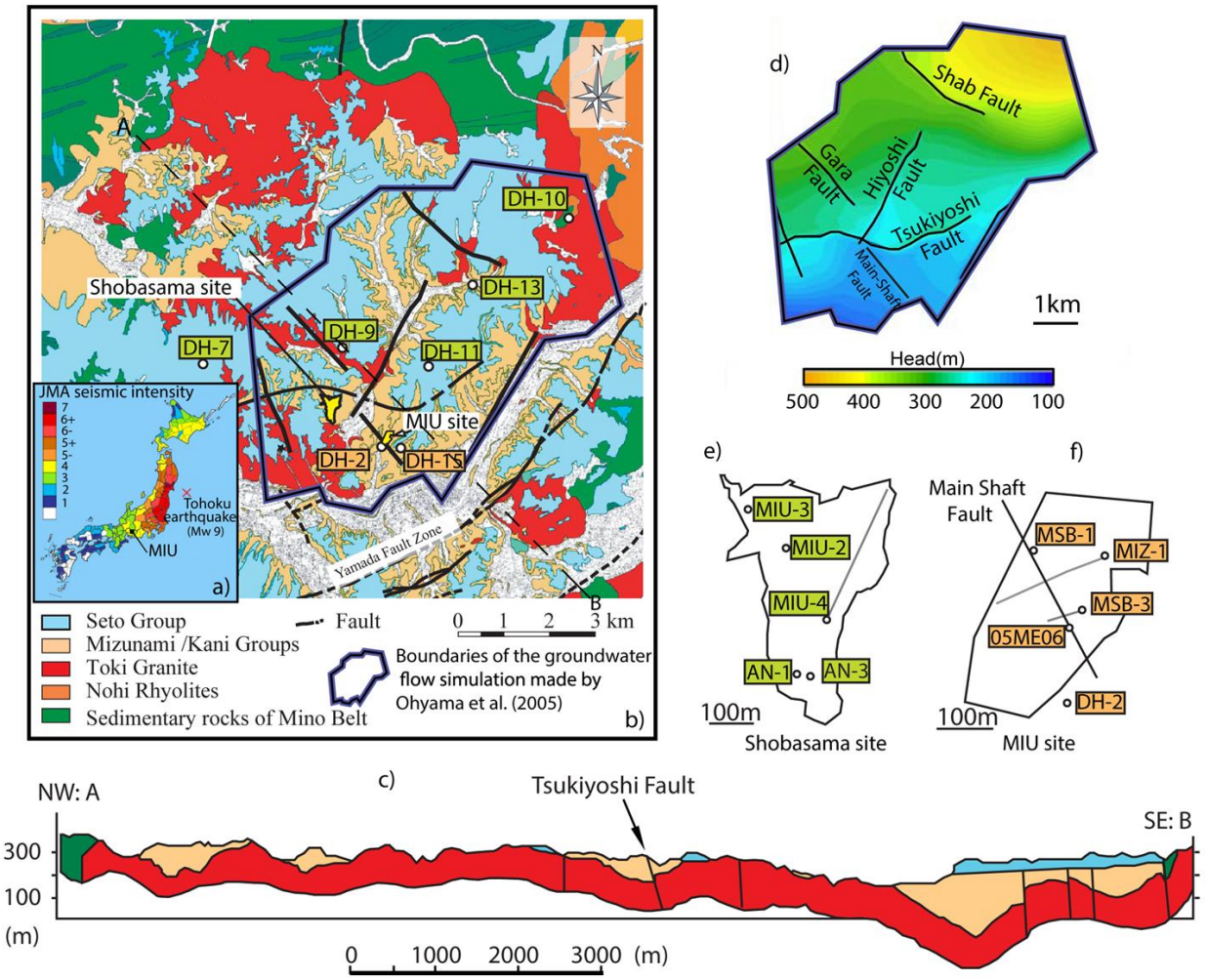

71

72 **Figure 1:** (a) Locations of the MIU site and the epicenters of the Tohoku Earthquake with a map of the
73 seismic intensity observations resulting from Tohoku Earthquake (Source: Japan meteorological agency).
74 (b and c) Geological setting near the MIU site (JNC TN7410 2003-001), with the location of the (e)
75 Shobasama and (f) MIU site with locations of groundwater monitoring boreholes (Niwa et al., 2012).
76 Boreholes in green and orange recorded respectively a decrease or an increase in groundwater level
77 during the day following the earthquake. (d) Hydraulic gradient in the study area calculated from a
78 groundwater flow simulation by Ohyama et al. (2005).

79

2. Hydrogeological context of the Mizunami Underground Research Laboratory

Japan Atomic Energy Agency (JAEA) is pursuing a geoscientific research and development project, namely the Mizunami Underground Research Laboratory (MIU) Project, in crystalline rock environment in order to construct scientific and technological basis for the geological disposal of high-level radioactive waste. The geology of the site is as shortly as follows: the basement granite called the 'Toki Granite' (late Cretaceous) and the overlying Mizunami Group (Miocene) 0 to 300 m in thickness (Fig.1c). In the frame of multidisciplinary research conducted in and around the MIU, groundwater pressures and levels were continuously recorded in several boreholes drilled from ground surface in and around the MIU (Fig.1). All the boreholes for groundwater monitoring were drilled into the Toki Granite, a Late Cretaceous intrusion. Depth of these boreholes ranges approximately from 200 m to 1300 m (Karino et al., 2011). Multiple piezometers were installed in each boreholes (except DH-15 and MIZ-1) between inflatable packers. In DH-15 and MIZ-1 a hydraulic pressure transducer was inserted in a standpipe connected to each measurement interval bounded by packers. All measurement intervals (except shallower parts of DH-15, MSB-1 and MSB-3) are in the granite, under in situ groundwater pressure conditions. The shallower parts of DH-15 are in the basal conglomerate lying on the unconformity between the Mizunami Group and Toki Granite, and the shallower parts of MSB-1 and MSB-3 are in the Miocene sedimentary rocks of the Mizunami Group (see Niwa et al., 2012). It should be noted that some very strange hydraulic head behavior can be caused by packer systems - especially when multiple different tests are done by packing off different intervals in a borehole (Smart, 1999). However, several arguments suggest that the observed changes in groundwater pressure presented in this study are not artifact: (1) the changes started with the arrival of the seismic waves generated by the Tohoku earthquake; and (2) all the multiple piezometers installed in each boreholes shown the exact same hydraulic behavior, excepted if the well intersected a major fault zone, and in this case two distinct behaviors can be observed in the hanging and in the footwall.

These multiple piezometers were installed to characterize (i) the regional groundwater flow, which is an important factor in the assessment of contaminant migration in deep underground and (ii) changes in the groundwater environment caused by excavation of shafts and galleries at the MIU site. In 2005, Ohyama et al. (2005) calculated the distribution of hydraulic gradient in the MIU area from groundwater flow simulation (Fig.1d). The authors show that the principal direction of groundwater flow in the area is from North-East to South-West, and that the groundwater flow is strongly affected by the Tsukiyoshi Fault, which is the most significant structure in the area. Indeed, the distribution of the hydraulic gradient is significantly different to North and South of the Tsukiyoshi Fault, which acts as a low permeability barrier on the groundwater flow (Fig.1d). The Hiyoshi Fault and the Shab Fault also seem to act as low permeability barriers on the groundwater flow with a higher hydraulic gradient on the West of the Hiyoshi Fault and on the East of the Shab Fault. Inversely, the Main-Shaft Fault seems not to have a significant influence on the regional hydraulic gradient. Then, the Mw 9.0 Tohoku Earthquake occurred off the Pacific coast on 11 March 2011 with observed changes in groundwater pressure in 15 boreholes drilled in and around the MIU (Fig.1).

3. Changes in groundwater pressure induced by the 2011 off the Pacific coast of Tohoku Earthquake

Niwa et al (2012) present in details the water pressure responses observed in 15 boreholes around the MIU site caused by the 2011 off the Pacific coast of Tohoku Earthquake. Here, we pay special attention to the monitored total head evolution relative to the main faults present in the area (the Tsukiyoshi Fault and the Hiyoshi Fault). We can observe that:

- North of the Tsukiyoshi Fault, the Tohoku earthquake caused a sharp drop in total head followed by a recovery period. Total head did not recover to its pre-earthquake state even after six months in boreholes located West of the Hiyoshi Fault (boreholes DH-7 and DH-9, Fig. 2a). East of the Hiyoshi Fault, on the other hand, the total head began to recover shortly after the earthquake and

eventually reached a higher level after a few months (boreholes DH-11 and DH-13, Fig. 2b).

- South of the Tsukiyoshi Fault, two behaviors were observed in the monitoring intervals present in the granite formation. At the Shobasama site the Tohoku earthquake also caused a sharp drop in total head in boreholes followed by a recovery period of for several months (boreholes AN-1, AN-3, MIU-2, MIU-3 and MIU-4, Fig. 2c). Inversely, at the MIU site, the earthquake causes a sharp increase in total heads (boreholes DH-2, DH-15, MSB-3, 05ME06 and MIZ-1, Fig. 2d).

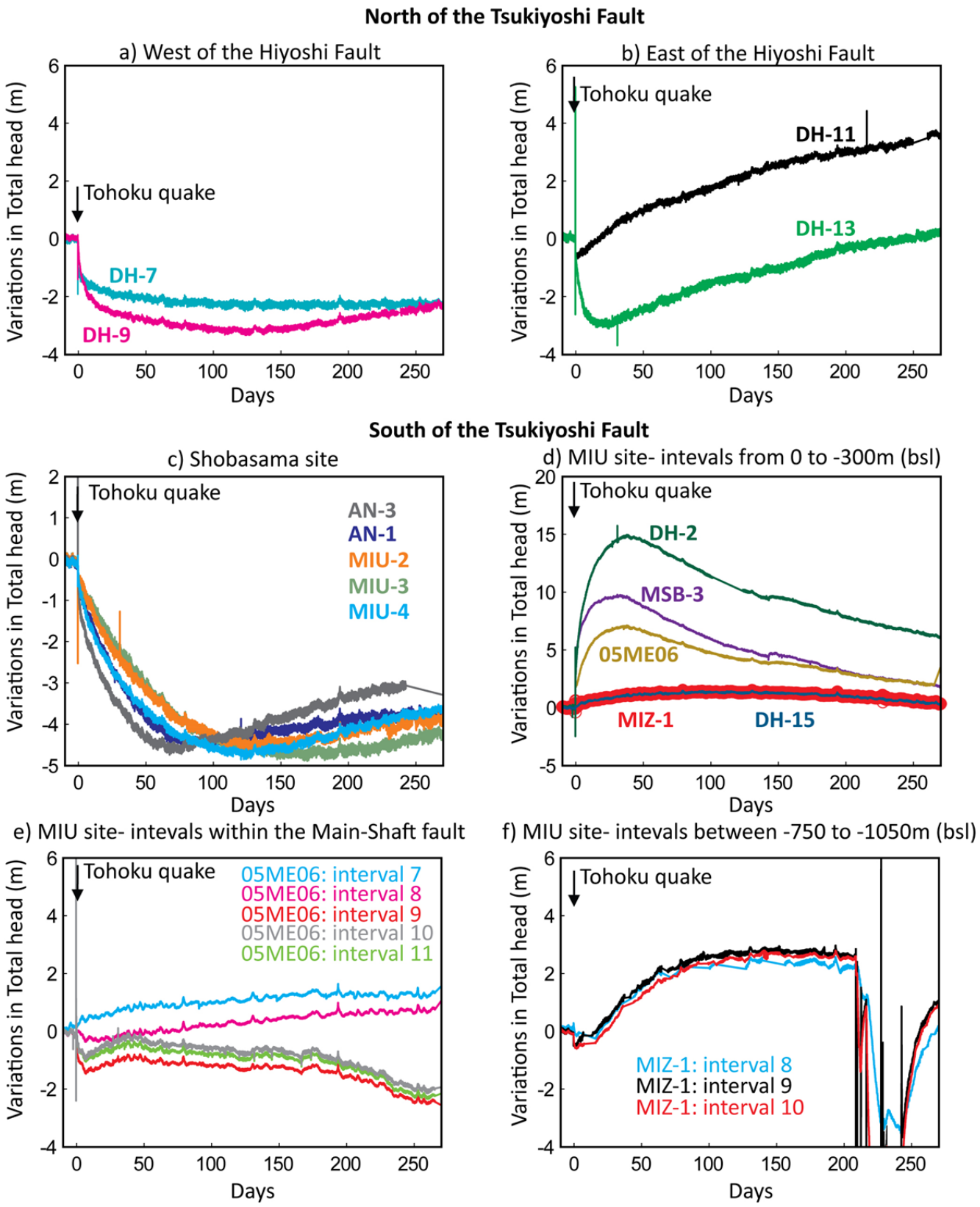

137

138 **Figure 2:** Representative examples of total head monitored in boreholes North of the Tsukiyoshi Fault

(a) West and (b) East of the Hyioshi Fault, and South of the Tsukiyoshi Fault (c) at the Shobasama site and (d) at the MIU site. Total head monitored at the MIU site (e) within the Main-Shaft Fault and (f) in the deepest intervals.

4. Fluid flow simulation

We performed numerical simulations with the fluid flow simulator TOUGH2 (Pruess et al., 2011). TOUGH2 is a general-purpose numerical simulation program for multi-dimensional fluid and heat flows of multiphase, multicomponent fluid mixtures in porous and fractured media. TOUGH2 solves mass and energy balance equations that describe fluid and heat flow in general multiphase, multicomponent systems. Fluid advection is described with a multiphase extension of Darcy's law; in addition there is diffusive mass transport in all phases. Heat flow occurs by conduction and convection, the latter including sensible as well as latent heat effects. The description of thermodynamic conditions is based on the assumption of local equilibrium of all phases. Fluid and formation parameters can be arbitrary nonlinear functions of the primary thermodynamic variables. Chief application areas are in geothermal reservoir engineering, nuclear waste isolation studies, environmental assessment and remediation, and flow and transport in variably saturated media and aquifers.

In this study, we used TOUGH2 to better understand the role and the behavior of the different fault zones present in the area on the observed groundwater pressure changes. We built a simplified geological model of the study area and performed a series of simulations to investigate (1) changes in permeability along the Tsukiyoshi Fault, the Hiyoshi Fault and the Main-Shaft Fault, (2) the influence of the shaft excavation and (3) the hydraulic connectivity between the sedimentary cover and the underlying granite.

4.1 Model set-up

We used the software package Groundwater Modeling System (GMS; Aquaveo, 2013) to build a 3D geological model. The grid was created using the 'grid approach' in GMS to generate a 3D structured

Voronoi grid. The grid convergence was reached and the grid was then linked to TOUGH2. GMS is a graphical user environment, which consists of a graphical user interface (the GMS program), providing tools for model conceptualization, mesh, and grid generation. Fault zones were also represented in these simulations, albeit simplified to follow the grid orientations. The 3D model is a simplified geological model, it was built by using:

- the map of the elevation of unconformity between Toki granite and Mizunami Group, determined by an electoromagnetic survey (JAEA-Research 2010-067, Final Report on the Surface-based Investigation Phase (Phase I)) (Fig.3a).
- geological logging from the borehole investigations at the regional hydrogeological scale, at the MIU site and at the Shobasama Site (JAEA-Research 2010-067, Final Report on the Surface-based Investigation Phase (Phase I)).
- The land digital elevation model (Fig.3b).

Based on these subsurface horizons and on borehole data, we used GMS to construct a regional three-dimensional geologic model including the MIU site and the Shobasama site. Our model includes, from the top down, the Mizunami Group that forms the sedimentary cover, the upper fractured granite, and the Toki granite that is assumed to extend deep downward.

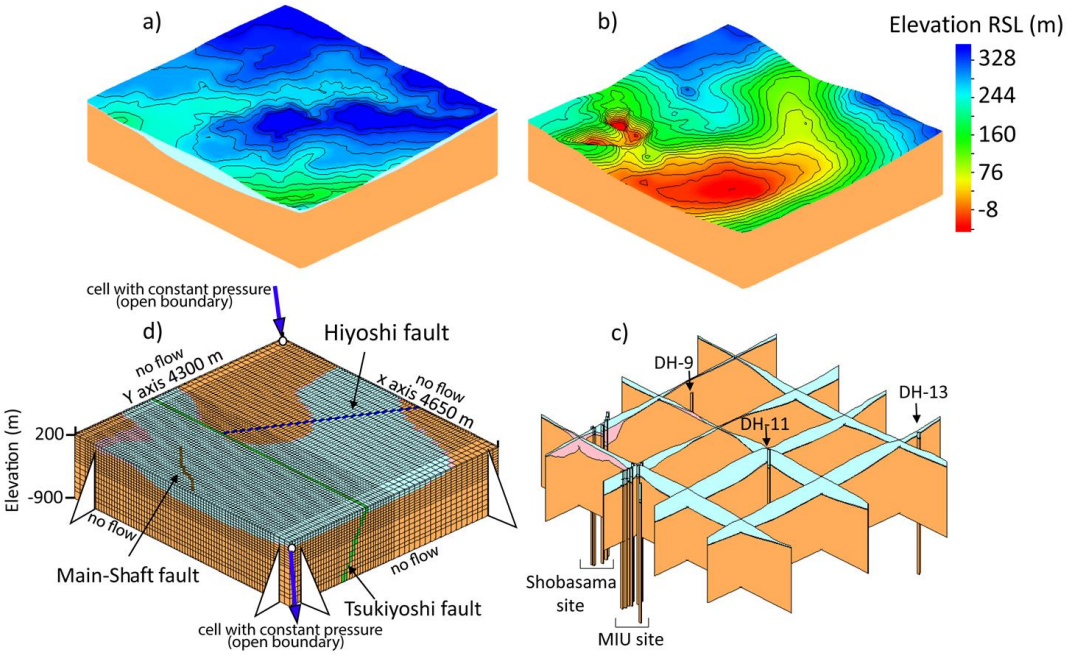

182

183 **Figure 3:** Simplified 3D geological model made from (a) the digital elevation model, (b) top of the Toki
184 granite (elevation Relative to Sea Level), and (c) borehole data. (d) 3D geological model and numerical
185 grid for fluid flow simulation with the Tsukiyoshi Fault (green), the Main-Shaft Fault (brown), the
186 Hiyoshi Fault (dark blue), the Toki granite (orange), the Mizunami sedimentary Group (light blue) and
187 the upper fractured granite (pink).

188

189 We then map this model onto a rectangular grid for use with the TOUGH2 numerical simulator (Fig.3d).
190 The numerical model extends vertically from 200 to -900 m (elevation relative to sea level) and
191 4650×4300 m horizontally. Finally, the Tsukiyoshi Fault and the Main-Shaft Fault are represented by
192 attributing different hydraulic properties to a set of cells. In our simulations, the Tsukiyoshi Fault is
193 oriented N090º-70ºS, the Hiyoshi Fault is oriented N030º-80ºE and the Main-Shaft Fault is oriented
194 N135º-90ºE.

195

4.2 Initial boundary conditions and initial parameters

First, we simulated a hydraulic gradient with a difference of 200m in water level between the Northwest and the Southeast by imposing a constant fluid pressure on the Northwest and the Southeast corners of our model (these two cells have open boundaries), however the other vertical boundaries have a "no flow" boundaries conditions (Fig. 3d). The bottom and top boundaries have "no flow" and "open flow" boundaries conditions respectively for multiphase flow. We also imposed a linear hydrostatic pressure gradient of 9.81 MPa/km ($\rho \times g \times h$, with ρ= density of the fluid, g= acceleration of gravity and h = depth) with depth and a constant temperature of 15ºC. These initial conditions are established through steady-state and multiphase flow simulations until a steady state was reached (Fig. 4a). In this case, we use the permeability and porosity for the different geological unit established through field investigation and numerical simulations (Table 1) (JAEA-Research 2010-067, Final Report on the Surface-based Investigation Phase (Phase I)). The faults have a lower permeability than the other geological formations and act as low permeable barriers between the North and the South fault compartments. Then, we simulated groundwater extraction at the MIU site to simulate the influence of the shaft excavation (Fig. 4b). Indeed, the boreholes near the MIU site have shown continuous drawdown since the shaft excavations started. For example, total heads have decreased approximately 35 m in MSB-1 and 87 m in MSB-3 (Niwa et al., 2012). In our simulation, we imposed a pumping rate of $6 m^3/s$ during three months to simulate a pressure drop of ~0.5MPa at the MIU site, which correspond to a decrease in total head of ~50m roughly in the range of the measured total head dropped.

Table 1: Hydraulic properties used during the simulations (JAEA-Research 2010-067, Final Report on the Surface-based Investigation Phase (Phase I))

	Porosity	Porosity after quake	Permeability x (m^2)	Permeability y (m^2)	Permeability z (m^2)
Fractured Granite	0.007	0.01	1.00E-13	1.00E-13	1.00E-13
Altered zone	0.01	0.03	3.22E-10	3.22E-10	1.61E-11
Sediment	0.20	0.22	2.56E-12	2.56E-12	2.51E-14
Tsukiyoshi Fault	0.05	0.05	1.00E-15	1.00E-15	1.00E-15
Hiyoshi Fault	0.05	0.05	1.00E-15	1.00E-15	1.00E-15
Main-Shaft Fault	0.05	0.05	1.00E-15	1.00E-15	1.00E-15

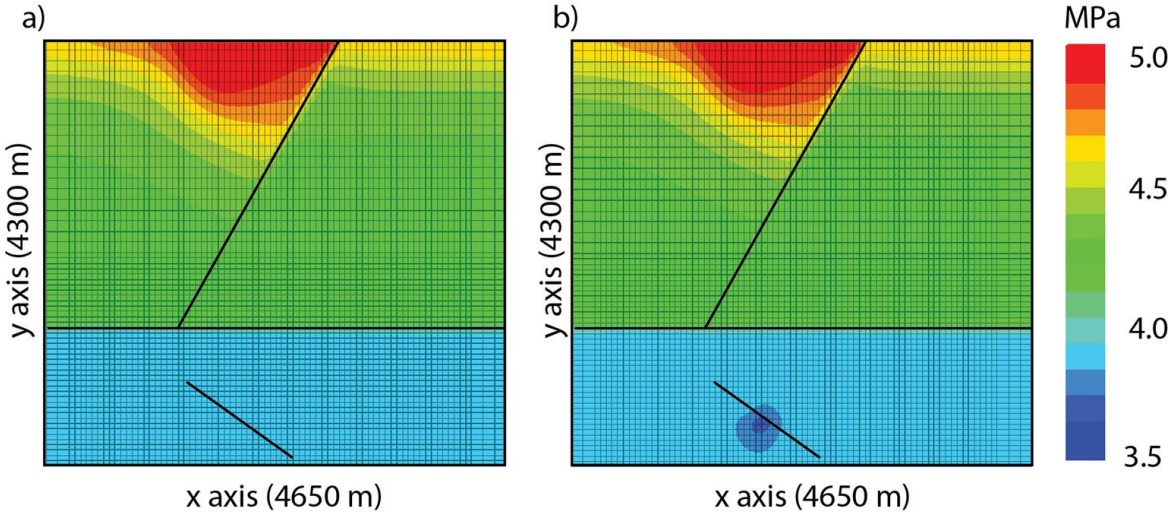

Figure 4: Simulated distribution of the hydraulic gradient between the Northwest and the Southeast influenced by the recharge through the sedimentary cover (Mizunami Group, see Fig. 2d), by (a) the influence of the three faults and by (b) groundwater extraction at the MIU site at ~500m deep.

4.3 Simulation of crustal dilation caused by the Tohoku earthquake

Niwa et al. (2012) calculated the volumetric strain changes at a depth of 1 km in Eastern Japan due to the Tohoku Earthquake using a dislocation analysis based on the theory of Okada (1992). They found approximately an amount of 2×10^{-7} dilation strain around the MIU site. Then, they calculated the theoretical amount of groundwater level changes due to this amount of crustal dilation (2×10^{-7}) associated with the Tohoku Earthquake and the tidal response in each borehole around the MIU site. In this way,

Niwa et al. (2012) found consistent results between the calculated and observed single-day drawdowns in the boreholes more than 1 km away from the MIU site associated with the Tohoku earthquake. This means that crustal dilation was one of the principal phenomenon responsible for the monitored changes in groundwater level.

To simulate this crustal dilation associated with the Tohoku earthquake we increased the porosity in each formation (see Table.1, porosity after quake) and the gas saturation (from 0 to 5%) in the water-saturated formations during the first time step of the fluid flow simulations. The gas saturation was increased because, in TOUGH2, if we increase the porosity and keep the liquid saturation constant (here 100%) more water will be added to our model. This behavior is unrealistic, indeed when a crack is created it doesn't lead to the creation of groundwater. So, to avoid this and to simulate crustal dilation by the sudden appearance of new unsaturated porous space we slightly increased the gas saturation when we increased the porosity. In this way, no additional water was added to the model and we were able to simulate groundwater flow from the saturated porous space to the newly created unsaturated porous space resulting in a drop in the water table, as observed in the field.

4.4 Influence of the changes in faults permeability

It is well known that fault zone are thick corridors with a complex structure that is classically described as composed of (1) a single or multiple core zone, and (2) a fractured damage zone (Chester et al., 1993). Typically, the fault-core permeability is two-to-three orders of magnitude lower than the host rock and may act as an impermeable barrier to fluid flow, whereas in the damage zone, the high fracture density make the damage zone more permeable than the host rock. However, all the complexity of fault zones has to be simplified in our regional flow model where the fault zones thickness are represented by only one cell. In our study, we chose to emphasis the role of the fault core and its impermeable behavior visible at the regional scale. For this reason, we chose to represent the fault zone with an initial very low isotropic permeability, and then with an higher isotropic permeability to simulate to allow fluid flow between the

two fault compartments.

So, we performed three fluid flow simulations in which the isotropic permeability of one of the faults was increased by two orders of magnitude (up to 10^{-13} m^2), considering or not the presence of a depression cone at the MIU site. We calculated changes in total head at six control points (CP) located where observation wells are approximately located in the field to compare monitored and calculated changes in total head.

North of the Tsukiyoshi Fault, we observe that:

- An increase in permeability along the Hiyoshi Fault causes a diffusion of the hydraulic gradient from the West to the East of the Hiyoshi Fault. This hydraulic diffusion results in a calculated drop in water level to the West (see CP-DH9 on Fig. 5a) and an increase to the East (see CP-DH11 and CP-DH13 on Fig. 5a). This behavior is similar to the field observations (see DH9, DH11 and DH13 on Fig. 2a and 2b).
- Inversely, an increase in permeability along the Tsukiyoshi Fault or along the Main-Shaft Fault fail to reproduce the observed data. Indeed, an increase in permeability along the Tsukiyoshi Fault causes the diffusion of the hydraulic gradient from the North to the South compartments of the Tsukiyoshi Fault and therefore results in a drop in total head everywhere in the North compartment (Fig. 5b). Whereas an increase in permeability of Main-Shaft Fault causes a slight decrease in total head at CP-DH11 and CP-DH13 due to the diffusion of the hydraulic gradient. (Fig. 5c).

South of the Tsukiyoshi Fault at the Shobasama site, we observed:

- An increase in permeability along the Tsukiyoshi Fault causes a diffusion of the hydraulic gradient from the North to the South leading to an increase in total head in the South compartment (Fig. 5e). So, to simulate the slow recovery observed at the Shobasama site following the Tohoku earthquake, the permeability of the Tsukiyoshi Fault has to stay unchanged (Fig. 5d or 5f).

- The presence of a depression cone at the MIU site has little effect on the calculated pressure level at the Shobasama site (compare Figs. 5d, e, f with Figs. 5g, h, i)

South of the Tsukiyoshi Fault at the MIU site, we observed:

- An increase in total head calculated at all the control points (CP-DH2, CP-DH15 and CP-MIZ1) located near the top of the Toki granite (~-240m bsl) in all the cases with or without the presence of a depression cone (Fig. 5j to 5o).
- A small drop in total head calculated in deeper control point (CP-MSB1, z = -840m bsl) calculated with or without a depression cone, when the permeability of the Tsukiyoshi Fault is unchanged (Fig 5j, 5l, 5m and 5o).

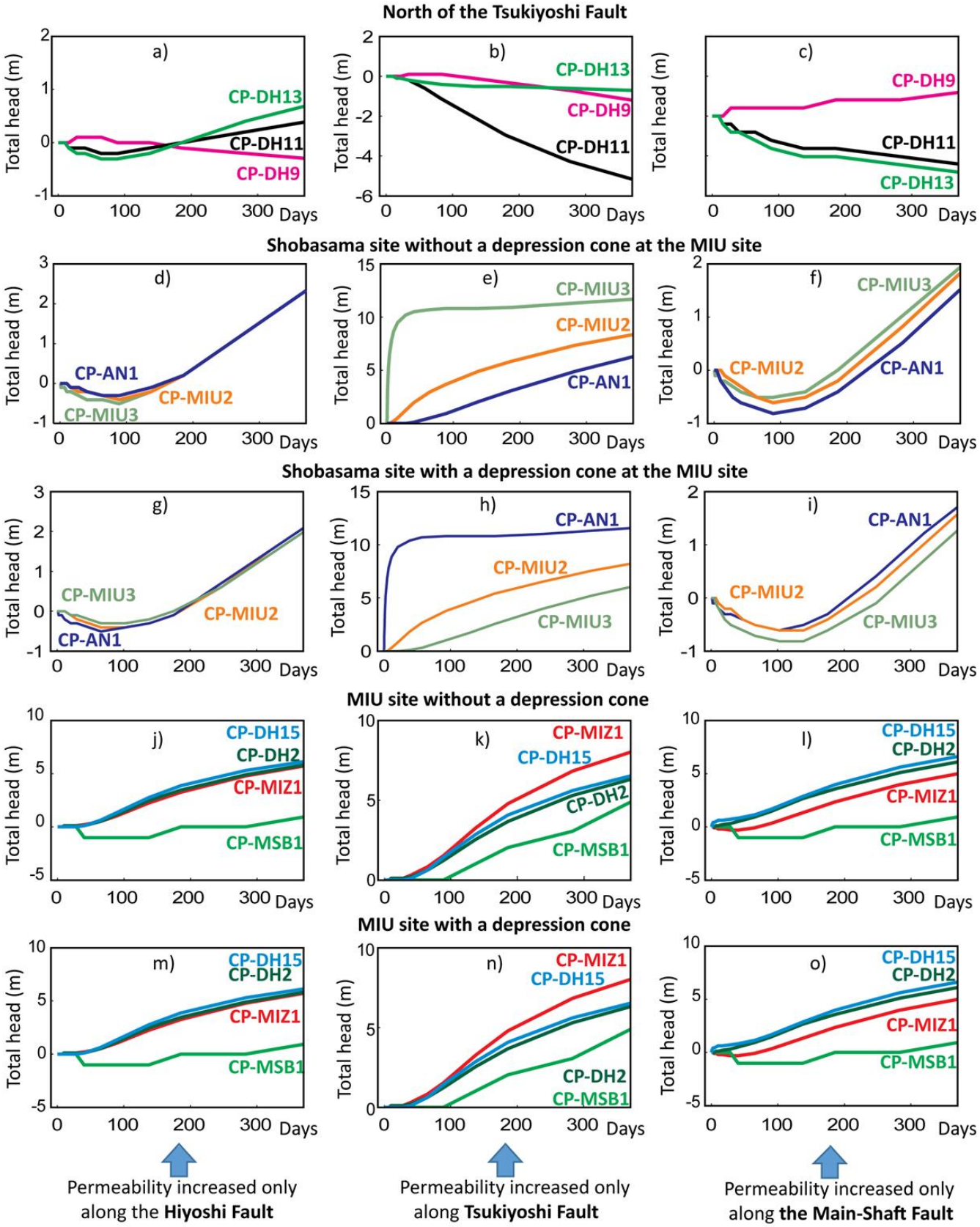

289

290 **Figure 5:** Simulation results showing the calculated total head evolution after the simulated crustal

dilation and changes in fault permeability along the Hiyoshi Fault (right column), along the Tsukiyoshi Fault (middle column) and along the Main-Shaft Fault (left column). Total head evolution (a to c) north of the Tsukiyoshi Fault, at the Shobasama site (d to f) without and (g to i) a depression cone at the MIU site, and at the MIU site (j to l) without and (m to o) a depression cone.

4.5 Sensitivity analysis on sedimentary cover permeability

The Toki granite is overlaid by sedimentary rocks that are aquifers containing large volumes of groundwater. To investigate how the hydraulic connectivity between these aquifers and the Toki granite aquifer may have influenced the monitored changes in groundwater pressure we conducted a new set of simulations where the vertical permeability in the sedimentary cover and in the altered zone were decreased (down to 10^{-16} m^2). As previously, we performed three fluid flow simulations where the permeability of one of the three faults was increased by two orders of magnitude (up to 10^{-13} m^2). Here, we did not simulate a depression cone at the MIU site. Results are shown in Figure 6. These simulations reveal a low influence of the vertical groundwater flow North of the Tsukiyoshi Fault on the calculated changes in groundwater pressure and a higher influence in the South of the Tsukiyoshi Fault. Indeed:

- North of the Tsukiyoshi Fault, the calculated total head (Fig. 6a to 6c) are very similar to those calculated with a higher vertical permeability in the formations above the Toki granite (Fig. 5a to 5c).
- At the Shobasama site, in case of no change in permeability along the Tsukiyoshi Fault, the recovery period is less than 200 days (Fig. 5g and 5i) and more than a year (Fig. 6d and 6f) in case of a high and lower vertical permeability in the upper formations, respectively.
- At the MIU site, despite the lower vertical permeability in the formations above the Toki granite, we still calculated a small increase in total head (2 to 3 time smaller than in case of a higher vertical permeability) at all the control points (CP-DH2, CP-DH-15 and CP-MIZ1) located near

the top of the Toki granite (Fig. 6g to 6h). Also, the higher the vertical permeability is the faster the groundwater level increase in the deepest part of the granite (see CP-MSB1 on Fig. 5m and 6g).

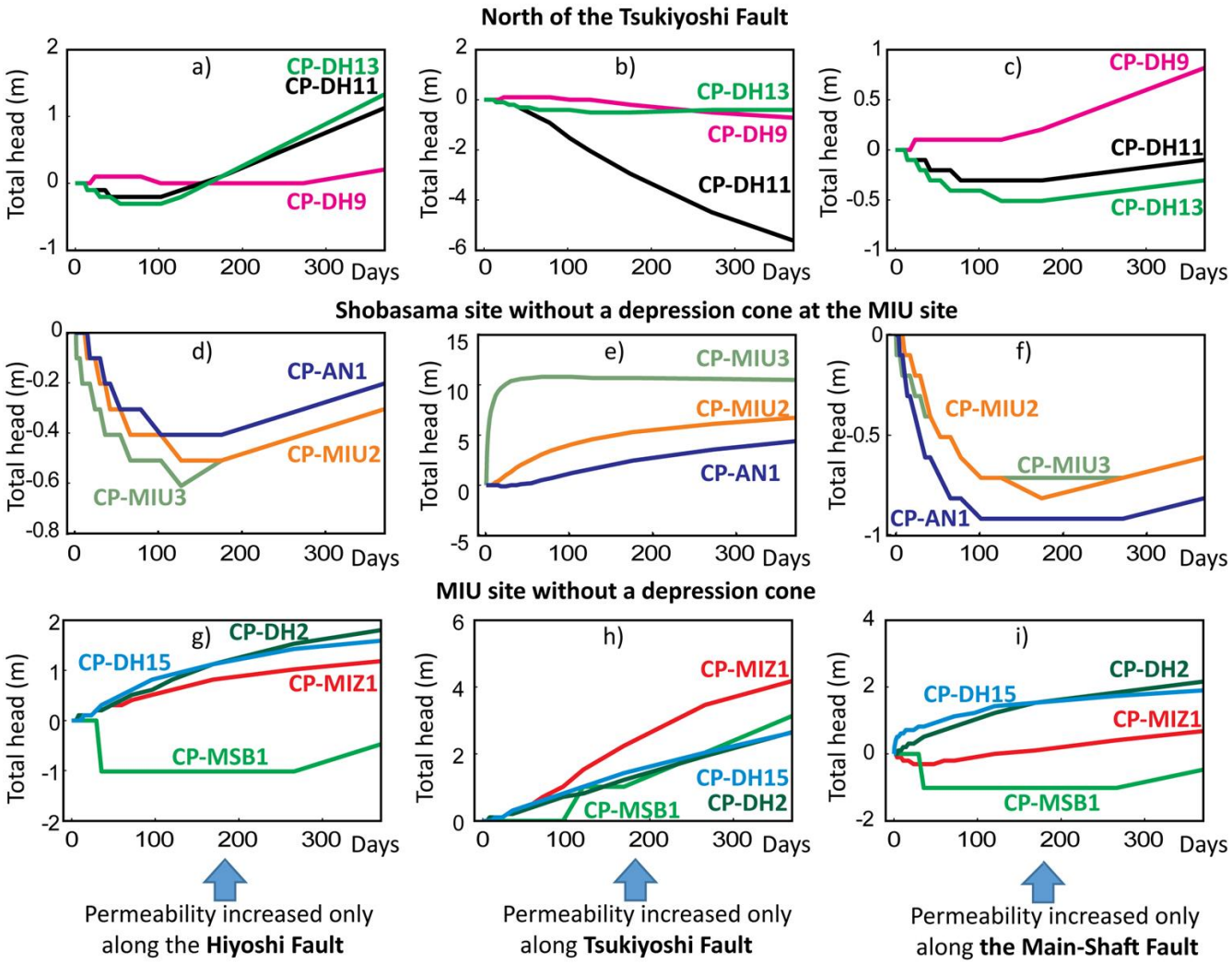

Figure 6: Simulation results showing the calculated total head evolution with a lower vertical permeability in the formation above the Toki granite after the simulated crustal dilation and changes in fault permeability along the Hiyoshi Fault (right column), along the Tsukiyoshi Fault (middle column) and along the Main-Shaft Fault (left column). Total head evolution (a to c) North of the Tsukiyoshi Fault,

at the Shobasama site (d to f) and (g to i) at the MIU site without a depression cone.

5. Discussion

5.1 Causes of changes in groundwater pressure

To understand the possible causes of the changes in groundwater pressure monitored in and around the MIU site due to the remote Tohoku earthquake, we have performed a series of fluid flow simulations to investigate the behavior of three faults present in the area and the role of the aquifers present in the sedimentary cover.

Our study indicates that the sudden increase in porosity within the rock formations due to crustal dilation led to:

- a vertical groundwater flow from the upper aquifers in the sedimentary cover to the deeper Toki granite. This is of particular importance at the MIU site where the sedimentary cover is thick (between ~150 to ~300 m). In this area, the general increase in total head seems to be mostly due to a flux of groundwater coming from the upper aquifers. Indeed, neither the presence of a depression cone nor an increase in permeability along the faults could explained the large increase in the monitored and calculated total head.
- This groundwater recharge from the upper aquifers to the Toki granite is smaller in areas with a thin sedimentary cover (between 0 to ~50m), as observed at the Shobasama site and North of the Tsukiyoshi Fault. In these cases, changes in groundwater pressure following the earthquake seems to be influenced by changes in permeability along low permeability faults.

Our study further indicates that only the permeability of the Hiyoshi Fault increased due to the Tohoku earthquake. Indeed:

- To reproduce the variations in total head monitored North of the Tsuhyioshi Fault and at the Shobasama site, the permeability along Hiyoshi Fault has to be increased, whereas the

permeability along the Tsukiyoshi Fault has to stay constant.

- As stated previously, there is no clear evidence that the changes in total head monitored at the MIU site were caused by an increase in permeability along the Main-Shaft Fault. On the contrary, the observed total head across the Main-Shaft Fault (Fig2.e) suggest the fault acted as a barrier to vertical groundwater flow. An increase in total head was observed in the upper part of the fault zone mostly due to a groundwater recharge from the upper formation (Fig2.e, intervals 7 and 8), and a decrease in the deeper part of the fault zone mostly due to an impermeable barrier within the fault zone (Fig2.e, intervals 9 to 11).

5.2 Causes of changes in fault permeability

Several explanations have been proposed to explain earthquake-induced changes in permeability along a fault in the intermediate and far field of an earthquake. The removal of gas from the pore space (Linde et al., 1994; Matsumoto and Roeloffs, 2003), the fracturing of solid rocks (Shi and Wang, 2016) and the removal of barriers clogging the groundwater flow (Brodsky et al., 2003) may cause such permeability variations. If one of these phenomena had occurred during the passing of seismic waves associated with the Tohoku earthquake it is hard to understand why it occurred only along the Hiyoshi Fault and not along the other faults. There are also a large number of observations showing that surface waves from remote earthquakes may trigger a slip along a pre-existing fault (Freed, 2005), and the fault reactivation could change its permeability. To see if the Tohoku earthquake was likely to induce slip along the faults in the vicinity of the MIU site we used the Mohr-Coulomb criterion (Jaeger and Cook, 2007). It provides an approximation of the shear and normal stresses acting on a fault, based principally on its orientation and the far-field stresses. For this reason, the Mohr-Coulomb criterion is the most commonly used criterion to describe fault stability in response to changes in shear stress and/or effective normal stress.

At the MIU site, at 500m depth the stress tensor was estimated to be a strike slip faulting regime with: $\sigma1$ = 21.3 MPa, $\sigma2$ = 12.7 MPa and $\sigma3$ = 11.7 MPa with maximum principal stress oriented NNW-SSE

(JAEA-Research 2010-067, Final Report on the Surface-based Investigation Phase (Phase I)). Under these conditions, we calculated the normal and shear stresses acting on the Hiyoshi Fault (N030-80E), the Main-Shaft Fault (135-90N), and on the three fault segments composing the Tsukiyoshi Fault (from West to East: N080-70S, N110-70S and N050-70S, see Fig.1). It appears that the Hiyoshi Fault and the Main-Shaft Fault are both critically oriented for shear reactivation (Fig.7). However, our simulation results indicates that changes in permeability occurred only along the Hiyoshi Fault. This different behavior between the two faults supposedly critically stressed may be caused by their different orientation and by the direction of the passing seismic waves generated by the Tohoku earthquake. Indeed, the seismic waves associated with the Tohoku earthquake propagated at the MIU site from the Northeast to the Southwest (Fig.1a). In case of the Main-Shaft Fault, the seismic waves propagated almost perpendicular to the fault potentially increasing the fault normal stress on the fault. Inversely, in case of the Hiyoshi Fault, the seismic waves propagated almost parallel to the fault potentially increasing the shear stress acting on the fault and favoring its reactivation. Northeast-Southwest

This last observation suggests the response of faults to dynamic loading by remote seismic waves depends on how favorably oriented towards stress they are and on the direction of propagation of seismic waves, which is in accordance with previous work (Hill, 2008). For example at the MIU site, seismic wave propagating in the Northeast-Southwest direction may trigger slip only along faults oriented ~N030 (e.g. the Hiyoshi Fault), whereas seismic wave propagating in the Northwest-Southeast direction may trigger slip only along faults oriented ~N135 (e.g. Main-Shaft Fault). We can also suppose that seismic wave propagating in the North-South or in the East-West directions do not trigger any slip along these two fault families.

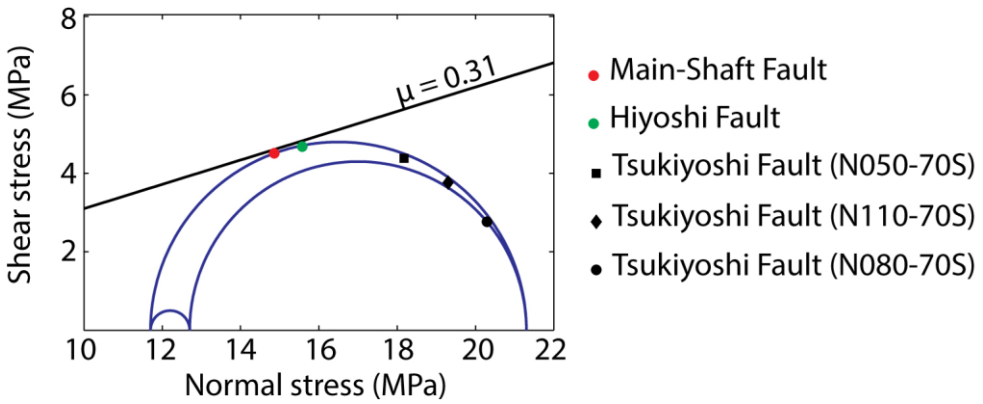

Figure 7: Mohr-circle diagram with the locations of the faults present in and around the MIU site.

6. Conclusion

We analyzed changes in groundwater pressure observed in several boreholes located in and around the Mizunami Underground Research Laboratory (MIU) induced by the 2011 Tohoku earthquake (Mw 9.0) to understand the behavior of the fault zones during the passing of seismic waves. Our results suggest that two main mechanisms are responsible for the observed changes in groundwater pressure: (1) crustal dilation induced by the Tohoku earthquake causing a groundwater recharge from the upper aquifers to the Toki granite in area where the sedimentary cover is thick; and (2) permeability increase along faults critically oriented for shear reactivation and oriented in the direction of the passing seismic wave. In this case, the seismic wave increases the shear stress acting on the fault promoting slip and a change in permeability. On the contrary, faults not critically stressed and faults critically oriented for shear reactivation but oriented perpendicular to the passing seismic wave are not reactivated.

Acknowledgments

The authors are deeply grateful to the Nuclear Waste Management Organization of Japan, who provided us the data. The work was conducted under U.S. Department of Energy contract No. DE-AC02-05CH11231 to the Lawrence Berkeley National Laboratory.

414

415 **References**

416 Aquaveo (2013), LLC in Provo, Utah. GMS User Manual (v9.0): The Groundwater Modeling System.

417 Blanchard, F.B.andByerly, P., 1935.Astudy of awell gauge as a seismograph, *Bull. seism. Soc. Am.,* **25,**

418 313–321.

419 Brodsky, E.E., Roeloffs, E., Woodcock, D., Gall, I. and Manga, M., 2003. A mechanism for sustained

420 groundwater pressure changes induced by distant earthquakes, *J. geophys. Res.,* **108,** 2390,

421 doi:10.1029/2002JB002321.

422 Cooper, H.H., Bredehoeft, J.D., Papadopulos, I.S. and Bennett, R.R., 1965. The response of well-

423 aquifer systems to seismic waves, *J. geophys. Res.,* **70,** 3915–3926.

424 Elkhoury, J.E., Brodsky, E.E.andAgnew, D.C., 2006. Seismic waves increase permeability, *Nature,* **441,**

425 1135–1138.

426 Freed, A., 2005, "Earthquake Triggering by Static, Dynamic and Postseismic Stress Transfer," *Annu. Rev.*

427 *Earth Planet. Sci.,* 33:335-67.

428 Geballe, Z.M., Wang, C.Y. and Manga, M., 2011. A permeability-change model for water-level changes

429 triggered by teleseismic waves, *Geofluids,* **11,** 302–308.

430 Hill DP (2008) Dynamic stresses, Coulomb failure, and remote triggering. Bul Seismo Soc Am

431 98:66-92.

432 JAEA-Research 2010-067, Final Report on the Surface-based Investigation Phase (Phase I) at the

433 Mizunami Underground Research Laboratory Project.

434 Jaeger, J., Cook, N., Zimmerman, R., 2007. Fundamentals of Rock Mechanics, 4th ed. Blackwell

435 Publishers, Oxford.

436 Jonsson, S., Segall, P., Pedersen, R. and Bjornsson, G., 2003. Post-earthquake ground movements

437 correlated to pore-pressure transients, *Nature,* **424,** 179–183.

JNC TN7410 2003-001, Master plan of the Mizunami underground research laboratory project, Tono Geoscience center Japan Nuclear Cycle Development Institute, February 2002.

Karino, T., H. Keya, and R. Takeuchi (2011), Data of long term hydro-pressure monitoring on Tono Regional Hydro-geological Study Project for fiscal year 2009, JAEA-Data/ Code 2011–001, Jpn. At. Energy Agency, Tokai, Japan.

Kitagawa, Y., Itaba, S., Matsumoto, N. and Koizumi, N., 2011. Frequency characteristics of the response of water pressure in a closed well to volumetric strain in the high-frequency domain, *J. geophys. Res.,* **116,** B08301, doi:10.1029/2010JB007794.

King, C.Y., Azuma, S., Igarashi, G., Ohno, M., Saito, H.andWakita, H., 1999. Earthquake-related water-level changes at 16 closely clustered wells in Tono, central Japan, *J. geophys. Res.,* **104,** 13 073–13 082.

Leggette, R.M. and Taylor, G.H., 1935. Earthquakes instrumentally recorded in artesian wells, *Bull. seism. Soc. Am.,* **25,** 169–175.

Lee M, Liu TK, Ma KF, Chang YM. 2002. Coseismic hydrological changes associated with dislocation of the September 21, 1999 Chichi earthquake, Taiwan. Geophys Res Lett. 29(17):5-1–5-4.

Linde, A.T., Sacks, I.S., Johnston, M.J.S., Hillt, D.P. and Bilham, R.G., 1994. Increased pressure from rising bubbles as a mechanism for remotely

triggered seismicity, *Nature,* **371,** 408–410.

Liu, L.-B., Roeloffs, E. and Zheng, X.-Y., 1989. Seismically induced water level fluctuations in the WaIi Well, Beijing, China, *J. geophys. Res.,* **94,** 9453–9462.

Matsumoto N. 1992. Regression analysis for anomalous changes of ground water level due to earthquakes. Geophys Res Lett. 19(12):1193–1196.

Matsumoto, N. and Roeloffs, E.A., 2003. Hydrological response to earthquakes in the HaibaraWell, central Japan. II: possiblemechanism inferred from time-varying hydraulic properties, *Geophys. J. Int.,* **155,** 899–913.

463 Niwa, M., R. Takeuchi, H. Onoe, K. Tsuyuguchi, K. Asamori, K. Umeda, and K. Sugihara (2012),
464 Groundwater pressure changes in Central Japan induced by the 2011 off the Pacific coast of
465 Tohoku Earthquake, Geochem. Geophys. Geosyst., 13, Q05020, doi:10.1029/2012GC004052.
466 Ohyama, T., Saegusa, H. and Onoe, H., 2005. “Groundwater Flow Analysis on Local Scale -Evaluation
467 of groundwater flow condition on Local scale and setting boundary conditions for groundwater
468 flow analysis on Site scale model in Step0-”, Japan Nuclear Cycle Development Institute, JNC
469 TN7400 2005-004. (in Japanese).
470 Okada, Y. (1992), Internal deformation due to shear and tensile faults in a half-space, Bull. Seismol.
471 Soc. Am. , 82, 1018–1040.
472 Piombo A, Martinelli G, Dragoni M. 2005. Post-seismic fluid flow and Coulomb stress changes in a
473 poroelastic medium. Geophys J Int. 162(2):507–515.
474 Pruess, K, Oldenburg, Moridis, G. 2011. TOUGH2 User’s Guide, Version 2.1, LBNL-43134(revised),
475 Lawrence Berkeley National Laboratory, Berkeley, California.
476 Quilty, E.G. and Roeloffs, E.A., 1997. Water-level changes in response to the 20 December 1994
477 earthquake near Parkfield, California, *Bull. seism.*
478 *Soc. Am.*, **87,** 310–317.
479 Roeloffs, E.A., 1998. Persistent water level changes in a well near Parkfield, California, due to local
480 and distant earthquakes, *J. geophys. Res.,* **03,**
481 869–889.
482 Rojstaczer, S.A. and Wolf, S.C., 1992. Permeability changes associated with large earthquakes; an
483 example from Loma Prieta, California, *Geology* **20,** 211–214.
484 Shi ZM, Wang GC, Liu CL, Mei JC, Wang JW, Fang HN. 2013. Coseismic response of groundwater
485 level in the three gorges well network and its relationship to aquifer parameters. Chin Sci Bull.
486 58(25):3080–3087.
487 Shi Z, Wang G. 2016. Aquifers switched from confined to semiconfined by earthquakes. Geophys Res

Lett. 43(21):11,166–11,172. doi:10.1002/2016GL070937.

Smart, C.C., 1999, Subsidiary conduit systems:A hiatus in aquifer monitoring and modeling, (in) Palmer, A. N., Palmer, M.V., and Sasowsky, I.D., (eds) Karst Modeling, Proceedings of the symposium held February 24 through 27, Charlottesville, Virginia, Karst Waters Institute Special Publication No.5, p. 146-157.

Sun X, Wang G, Yang X., 2015. Coseismic response of water level in Changping well, China, to the Mw 9.0 Tohoku earthquake. J Hydrol. 531:1028–1039.

Wang, C., and Chia, Y., 2008. *Mechanism of water level changes during earthquakes: Near field versus intermediate field,* Geophys. Res. Lett., *35*(12), L12402.

Wang, C.-Y. And Manga,M., 2010. *Earthquakes andWater,* Vol. **114,** Springer, 225 pp.

Wakita, H., 1975. Water wells as possible indicators of tectonic strain, *Science,* **189,** 553–555.

Xue L, Brodsky EE, Erskine J, Fulton PM, Carter R. 2016. A permeability and compliance contrast measured hydrogeologically on the San Andreas fault. Geochem Geophys Geosyst. 17(3): 858–871.